

A terahertz-driven electron gun

W. Ronny Huang¹, Emilio A. Nanni¹, Koustuban Ravi¹, Kyung-Han Hong¹, Liang Jie Wong¹, Phillip D. Keathley¹, A. Fallahi², Luis Zapata², and Franz X. Kärtner^{1,2,*}

¹*Department of Electrical Engineering and Computer Science and Research Laboratory of Electronics, Massachusetts Institute of Technology, Cambridge, Massachusetts 02139, USA*

²*Center for Free-Electron Laser Science, DESY and Department of Physics, University of Hamburg, Hamburg 22607, Germany*

*Corresponding author. Email: kaertner@mit.edu.

Electron sources at keV-MeV energies are indispensable for applications such as ultrafast electron diffraction¹, x-ray generation², and electron energy-loss spectroscopy³. However, the accessibility and size of current accelerators based on radio-frequency (RF) technology are limited by the achievable electric fields. Terahertz based accelerators promise unprecedented compactness compared to current RF accelerators due to the intense electric fields that can be applied in the accelerating structures. Here, electron bunches of 50 fC from a flat copper photocathode are accelerated from rest to a mean energy of 18 eV by a single-cycle THz field with peak electric field gradient of 72 MV/m at 1 kHz repetition rate. Scaling of the THz field into the gigavolt per meter regime^{4,5} would translate to electron energies of ~100 keV. Furthermore, in combination with the recent demonstration of a THz linear accelerator (linac)⁶, this is a milestone toward a millimeter- to centimeter-scale relativistic electron source.

The realization of a compact electron gun requires very intense electric fields in order to achieve electron bunches with high charge density, good beam quality, and large kinetic energy. Conventional guns powered by DC fields reach their performance limit at 10 MV/m due to field emission breakdown⁷, while guns powered by radio-frequency (RF) fields operate at 50-110 MV/m due to plasma breakdown

limitations⁸. Since the plasma breakdown threshold scales as the square root of the frequency⁹, there has been a great interest in the development of compact accelerators operating in higher-frequency regions of the electromagnetic spectrum^{10,11}. Near-infrared (NIR) laser pulses are one option because of their high fields (multi-GV/m), accessibility, and relatively low cost sources. Various NIR acceleration schemes have been investigated based on dielectric structures^{12,13}. However, due to the short NIR wavelength, phase matching between the electromagnetic field and electron, space charge effects, limited charge density, and fabrication of accelerating structures present challenging hurdles. Laser plasma wakefield acceleration has achieved GeV electrons¹⁴⁻¹⁶ using 100 TW - PW laser sources at low repetition rates with percent-level energy spread and jitter. Accelerators employing radiation at THz frequencies hold promise because of their long wavelength and high field breakdown threshold. Furthermore, the advent of efficient THz generation techniques¹⁷⁻²⁰ has made THz based accelerators a realistic possibility and has motivated studies for using THz radiation in improving electron energy and beam properties in high-brightness linacs^{21,22} and proton post-accelerators²³.

Thus far, keV electron acceleration of semi-relativistic electron bunches in a centimeter-long THz waveguide linac has been demonstrated⁶. To fully exploit the capabilities of THz radiation, acceleration from rest to keV levels and beyond, i.e. a THz electron gun, is also required. In this regard, very recently Li and Wimmer demonstrated THz acceleration from excited atoms²⁴ and an isolated nanotip²⁵, respectively. Their work, however, was geared toward understanding low-charge (<0.1 fC) electron emission dynamics from atoms and nanostructures.

In this paper, a mean acceleration of 18 eV on 50 fC electron bunches with a single-cycle 72 MV/m THz field (ponderomotive energy of 28.5 eV) is demonstrated. The acceleration of the above charge from rest qualifies the presented work as a proof-of-concept for a THz electron gun. The experimentally obtained acceleration results are well described by 3D particle tracking simulations. The electrons are emitted from a flat copper photocathode, akin to those used in conventional accelerators (e.g. LCLS²⁶) and well suited to high-electron-brightness applications due to its simplicity and robustness.

In the experiment, schematic and photograph shown in Figs. 1(a) and 1(b), an emit-and-accelerate scheme is employed on a flat copper photocathode. Electrons are emitted by two-photon ionization at the photocathode using a 525 fs pulse at 515 nm (green). The electron bunches were produced at 1 kHz repetition rate with a total charge per bunch of 50 fC. The photocurrent was measured at the photocathode. The emitted electrons were exposed to a p-polarized, single-cycle THz pulse with a carrier frequency of 0.45 THz (Fig. 2(a)). The reflection from the photocathode increases the THz field twofold. The THz pulse delivered onto the copper is focused to a beam waist of 1.1 mm (Fig. 1(c)) and has a final energy of 6 μ J with a calculated peak electric field on the surface of 72 MV/m.

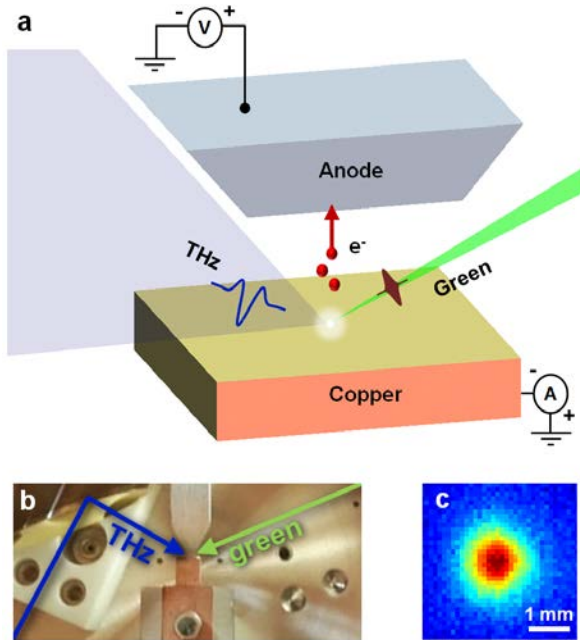


Figure 1 | Experimental setup. (a) Electrons are emitted from a flat copper cathode by a 525 fs green (515 nm) pulse and accelerated by a p-polarized single-cycle terahertz pulse. Electron spectrum information is obtained by applying a retarding bias and measuring the photocurrent. (b) Photograph of apparatus inside a vacuum chamber. (c) Terahertz beam intensity profile at the focus.

To provide basic understanding of the electron dynamics before describing experimental results, we present in Fig. 2 a simulation of emission and acceleration by a single-cycle THz field for our experimental conditions. Figure 2(a) shows the THz field at the photocathode surface as a function of time. The time-energy evolution of a single electron exposed to that field is shown in Fig. 2(b) for two THz field values. Emission occurs at -0.47 ps, the first node of the THz electric waveform where the field switches from positive to negative (green dots in Fig. 2(a)-(c)). Shortly after emission, for a THz field of 72 MV/m (blue curve), the electron is accelerated to 120 eV by the main negative half-cycle of the THz waveform (-0.47 to 0.47 ps) and thereafter decelerated to 26 eV by the final positive half-cycle (0.47 – 1.43 ps). Figure 2(c) shows the time evolution of the energy spectrum for an electron bunch of 50 fC. Due to the large pulse duration of the electron bunch, some electrons are emitted at the wrong time and therefore gain less energy. At long time scales, space charge forces cause leading/trailing electrons to gain/lose energy, resulting in a chirped energy spectrum. The final average energy of the electrons is 26 eV and the peak energy is 90 eV owing to space charge (Fig. 2(d)). The red curve in Fig. 2(b) shows that with a 2 GV/m field (twofold enhancement by reflection of a 1 GV/m field, corresponding to recent demonstrations^{4,5}), it is possible to achieve an average energy of 30 keV.

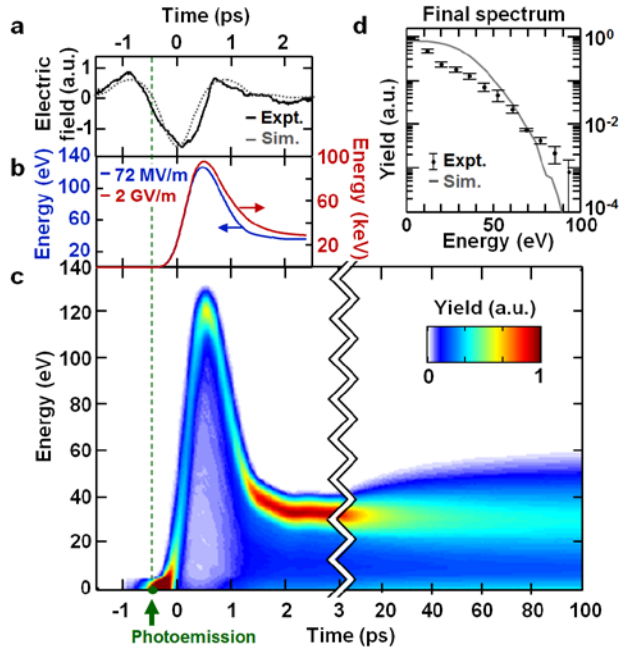


Figure 2 | Electron acceleration in a single-cycle terahertz field. (a) Electro-optic sampling trace of terahertz pulse. (b) Single-electron energy evolution in time. After emission (indicated by the green dashed line), the electron is accelerated by the negative half-cycle of the THz electric field and thereafter decelerated by the final positive half-cycle. Energy gained from a 72 MV/m field is 26 eV. With a 2 GV/m field (twofold enhancement of 1 GV/m fields, corresponding to recent demonstrations^{4,5}), it is possible to achieve 30 keV. (c) 50 fC electron bunch energy evolution under a 72 MV/m THz field showing the effect of finite electron bunch duration and space charge. At long time scales, space charge induces an energy chirp on the spectrum. (d) The final energy spectrum (gray line, simulation; black dots with one sigma error, experiment) shows an average energy of 26 eV (18 eV in experiment) with a peak energy of 90 eV (92 eV in experiment). Experimental data discussed further in Fig. 3(a).

The performance of the THz gun was determined by the electron energy spectra of the emitted electron bunch. The electron energy spectra were measured by varying the DC bias and recording the photocurrent at various points of delay between the green and THz pulse. At reverse biases, the DC field acts as a highpass filter for the photocurrent and therefore allows the measurement of the yield of electrons above an energy equal to the reverse bias, revealing electron energy spectral information. This setup essentially functions like a retarding field spectrometer without a field screen.

In Fig. 3(a), the experimentally measured photocurrent is plotted as a function of delay and bias voltage for 0, 36, and 72 MV/m THz field strengths. Note, a positive delay corresponds to the situation where the THz pulse arrives after the green pulse and vice versa. At a delay of 0.25 ps at 72 MV/m, we observe photocurrent modulation up to -92 V bias, indicating that a fraction of electrons achieved a peak energy of 92 eV to overcome the potential barrier, while the mean energy was measured to be 18 eV. This is in good agreement with the simulations shown in Fig. 2(c) that predict a peak energy of 90 eV and a mean energy of 26 eV.

The pulsewidth of emission is 17% of the THz carrier period and is therefore capable of revealing THz electric field phase-dependent effects. Figure 3(b) plots the photocurrent as a function of delay at a fixed bias voltage of -0.1 V. A similarity between the photocurrent trace and the integrated THz field is observed. Given the fact that the photocurrent is proportional to the average electron energy in this bias regime, the data reflects that the electron momentum gain is governed by the vector potential, $p_{gain} = -eA = -e \int_{t_{emit}}^{\infty} E(t') dt'$.

In Fig. 3(c), we compare the bias sweep with THz OFF and THz ON at a delay of 0.25 ps. We observe a significant rise of photocurrent at reverse biases up to ~ 30 V in the THz ON case, indicating clear evidence of THz acceleration. The energy spectra, shown in Fig. 3(d), were obtained by taking the derivative of the photocurrent with respect to bias voltage. The experimental data are verified by particle tracking simulations incorporating the bias field. While the simulation agrees well with experiment in the case of THz OFF, it slightly underpredicts the peak energy in the case of THz ON. This can be attributed to local hotspots on the photocathode due to surface nonuniformities or discrepancies arising from the macroparticle approximation (see Methods). Given the simplicity of the model, the agreement is satisfactory enough to explain the main features of the experimental results.

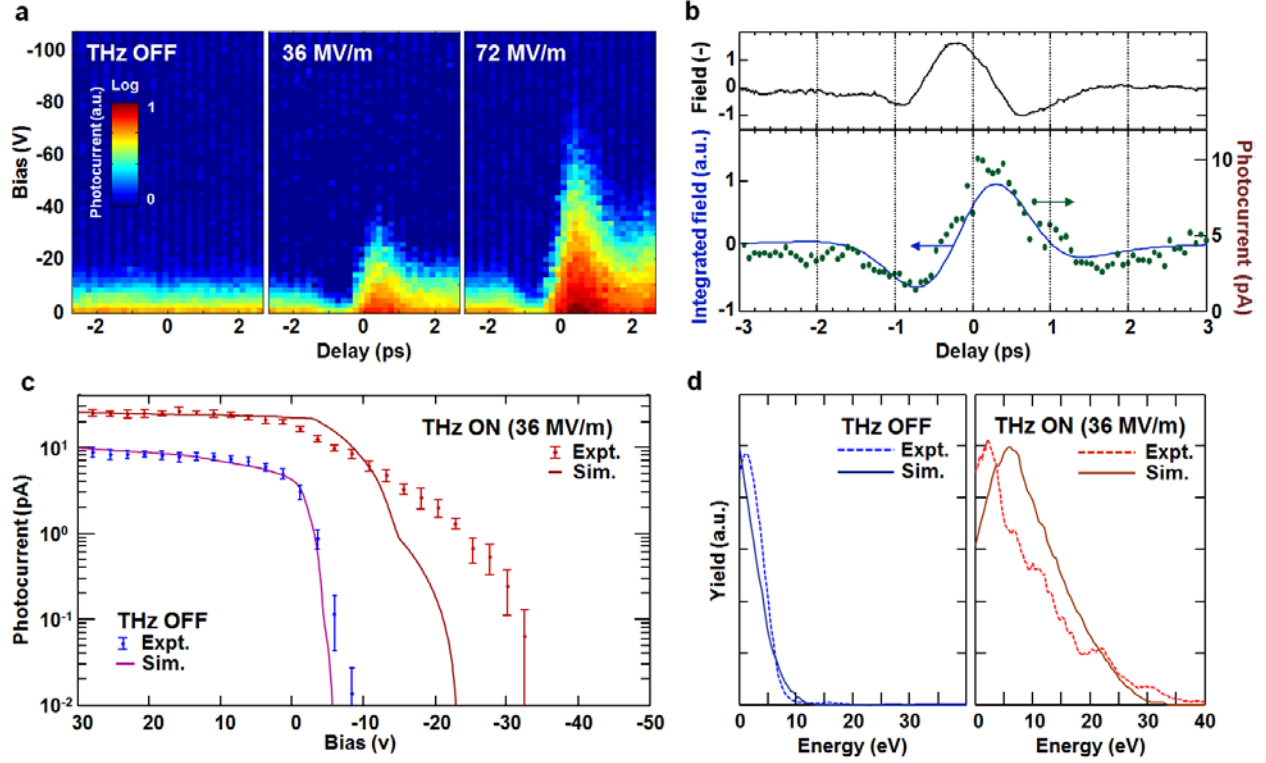


Figure 3 | Experimental evidence of terahertz-driven electron acceleration. (a) Spectrograms showing electron acceleration at various THz field intensities. At 72 MV/m, we observe an increase of photocurrent at reverse biases up to -92 V, indicating that electrons achieved a peak energy of 92 eV to overcome the potential barrier. (b) Experimental correlation between the photocurrent and integrated terahertz field reflects that the acceleration is governed by the vector potential. The bias here is set to a regime where the photocurrent is proportional to the electron energy. (c) Bias sweeps of photocurrent (dots with one sigma error bar) show a significant rise in photocurrent at strong reverse biases indicating clear evidence of THz acceleration. (d) Electron energy spectra comparing THz OFF and THz ON (36 MV/m).

In conclusion we have constructed a first version of a compact THz-driven electron gun. From a simple flat copper photocathode, we showed THz-driven acceleration of a 50 fC electron bunch from rest to a mean energy of 18 eV and peak energy of 92 eV using a 72 MV/m THz field at 1 kHz repetition rate. The demonstrated electron acceleration results are also in agreement with particle tracking simulations. This

simple scheme of employing a flat photocathode has promising scalability to larger bunch charge and higher THz surface fields due its high field breakdown threshold compared to RF or DC guns. Since bulk copper can withstand >1 GV/m of field strength at THz frequencies^{27,28}, THz acceleration using a flat copper photocathode is scalable by orders of magnitude in field strength without risk of optical damage. While the demonstrated acceleration is relatively modest, this experiment illustrates the potential of using THz fields for the development of electron guns. With scaling to a 1 GV/m THz field and shorter photoemission laser pulses (20 fs, or $T_{\text{THz}}/100$), this technique can yield low-emittance, monoenergetic electrons with energies up to 30 keV, suitable for ultrafast electron diffraction. In combination with recent scaling of THz electric field strengths and THz waveguide linacs, the presented work paves the way for the development of an all-optical, ultracompact, high repetition rate multi-MeV beamline.

Methods

Terahertz beam. The THz pulses are generated by optical rectification (OR) of tilted-pulse-front NIR pulses in cryogenic lithium niobate (LN). Up to 12 μJ THz pulse energy is generated with a conversion efficiency of about 1.0% at the crystal^{17,18}. The diverging THz beam is collimated by a 50.8 mm high-density polyethylene lens, converted from s- to p-polarization by a periscope, coupled into the vacuum chamber, and focused onto the photocathode by a parabolic mirror with an effective focal length of 25.4 mm. The THz beam is incident onto the photocathode at an angle of 67° (largest angle by which a f/1 focused beam can be incident on a flat surface without clipping). The large angle of incidence maximizes the electric field component normal to the photocathode surface.

The THz pulse is temporally characterized by a standard electro-optic (EO) sampling setup employing a 200 μm thick, 110-cut ZnTe crystal. 70 fs NIR pulses from the mode-locked fiber oscillator (see Pump source) sample the THz field-induced birefringence as a function of delay. A quarter-wave plate followed by a polarizer converts the field-induced birefringence to an intensity modulation, and the intensity modulation is recorded by a photodiode. The measured pulse has a carrier frequency of 0.45 THz and a

FWHM bandwidth of 0.4 THz. The THz beam was characterized spatially by a pyroelectric detector array (Spiricon Pyrocam III).

Pump source. The pump source for THz generation is a Yb:KYW chirped pulse regenerative amplifier (RGA) producing 1.5 mJ pulses with 1 kHz repetition rate at a near-infrared (NIR) center wavelength of 1030 nm and bandwidth of 2.1 nm. The dielectric grating compressor following the RGA compresses the pulses to a transform-limited pulse duration of 750 fs. The seed for the RGA was a mode-locked Yb-doped fiber oscillator emitting 70 fs, 0.2 nJ pulses at 80 MHz amplified to 1.6 nJ by a Yb-doped fiber amplifier²⁹. After losses through the optical elements in the setup, the impinging pump energy into the (LN) crystal was 1.2 mJ.

Photoemitter. About 2% of the available NIR pump energy was used to generate the green photoemitter pulses by second harmonic generation in a 0.75 cm long BBO crystal. A BG-39 bandpass filter was used to remove the fundamental NIR component. The green pulses have a pulsewidth of 525 fs and are focused at an angle of 67° onto the photocathode with a beam waist of ~50 μm. Since the emitted charge scales as the green pulse's intensity squared due to two-photon ionization, the effective duration of the electron bunch at emission is estimated to be lower than the duration of the green pulse approximately by a factor of $\sqrt{2}$, corresponding to 375 fs. Since both the THz and green pulses are produced from the same sub-ps NIR laser, the timing jitter between them is negligible.

Anode and cathode. A Poisson equation solver (Superfish³⁰) was used to model the static DC electric potential between the anode and cathode and it confirmed that the bias field is uniform over the emission area. Varying the DC bias between the cathode and anode does not impact the electron dynamics during the exposure to the THz field for two reasons. First, the bias was swept over +/- 110 V, corresponding to a DC field of +/- 52 kV/m, which is more than three orders of magnitude weaker than the THz field. Second, during the transient interaction with the THz pulse on the picosecond timescale, the electron dynamics are dominantly governed by the THz field.

Simulations. A particle tracking simulation was implemented to model the evolution of an electron bunch in the presence of the THz field. The initial electron bunch had a Gaussian spatial profile with beamwaist of 50 μm and a Gaussian temporal profile with FWHM of 375 fs. The initial kinetic energy was 0.18 eV (green two-photon energy subtracted by the copper work function) and the initial velocity vectors were uniformly distributed over a hemisphere. The particles were released 0.1 nm away from the surface. 6000 macroparticles were used to represent a total bunch charge of 50 fC, corresponding to a charge of $52e^-$ per macroparticle, where e^- is the unit charge. The trajectories were modeled by integrating the following system of differential equations for every particle i using a 4th order Runge-Kutta solver.

$$m \frac{dv_i}{dt} = \mathbf{F}_{field} + \mathbf{F}_{bias} + \mathbf{F}_{image,i} + \sum_j \mathbf{F}_{ij}$$

$$\frac{dr_i}{dt} = \mathbf{v}_i$$

Here, m is the relativistic mass, \mathbf{F}_{field} is the electric force due to the THz pulse, \mathbf{F}_{bias} is the electric force due to the DC bias, $\mathbf{F}_{image,i}$ is the image charge force on the i^{th} particle due to the bulk metal cathode, and \mathbf{F}_{ij} is the particle-particle Coulomb force. The THz beam was modeled as a fundamental Gaussian beam with numerical aperture of 1/2. The THz pulse spectrum was directly adapted from that obtained by EO sampling with a flat spectral phase profile.

References

- [1] Baum, P. & Zewail, A. H. Breaking resolution limits in ultrafast electron diffraction and microscopy. *Proc. Natl. Acad. Sci. U. S. A.* 103, 16105–10 (2006).
- [2] McNeil, B. W. J. & Thompson, N. R. X-ray free-electron lasers. *Nat. Photonics* 4, 814–821 (2010).
- [3] Egerton, R. F. Electron energy-loss spectroscopy in the TEM. *Reports Prog. Phys.* 72, 016502 (2009).
- [4] Vicario, C., Monoszlai, B. & Hauri, C. P. GV/m Single-Cycle Terahertz Fields from a Laser-Driven Large-Size Partitioned Organic Crystal. *Phys. Rev. Lett.* 112, 213901 (2014).

- [5] Shalaby, M. & Hauri, C. P. Terahertz brightness at the extreme: demonstration of 5 GV / m low frequency λ 3 terahertz bullet. arXiv:1407.1656 (2014).
- [6] Nanni, E. A. et al. Linear electron acceleration in THz waveguides. International Particle Accelerator Conference, WEOAB03, (2014).
- [7] Loehl, F. et al. High current and high brightness electron sources. in Proc. IPAC'10, Kyoto, Japan 45–49 (2010).
- [8] Spataro, B. et al. Technological issues and high gradient test results on X-band molybdenum accelerating structures. Nucl. Instruments Methods Phys. Res. Sect. A Accel. Spectrometers, Detect. Assoc. Equip. 657, 114–121 (2011).
- [9] Loew, G. A. & Wang, J. W. RF breakdown studies in room temperature electron linac structures. in 13th Int. Symp. Discharges Electr. Insul. Vacuum, Paris, Fr. (1988).
- [10] Braun, H., Döbert, S., Wilson, I. & Wuensch, W. Frequency and Temperature Dependence of Electrical Breakdown at 21, 30, and 39 GHz. Phys. Rev. Lett. 90, 224801 (2003).
- [11] Brown, W. J. et al. "Experimental and theoretical investigations of a 17 GHz RF gun." *Nuclear Instruments and Methods in Physics Research Section A: Accelerators, Spectrometers, Detectors and Associated Equipment* 425, 441-459 (1999).
- [12] Peralta, E. A. et al. Demonstration of electron acceleration in a laser-driven dielectric microstructure. Nature 503, 91–4 (2013).
- [13] Breuer, J. & Hommelhoff, P. Laser-Based Acceleration of Nonrelativistic Electrons at a Dielectric Structure. Phys. Rev. Lett. 111, 134803 (2013).
- [14] Faure, J. et al. A laser–plasma accelerator producing monoenergetic electron beams. Nature 431, 541–544 (2004).

- [15] Leemans, W. P. et al. GeV electron beams from a centimetre-scale accelerator. *Nature Phys.* 2, 696–699 (2006).
- [16] Hafz, A. M. et al. Stable generation of GeV-class electron beams from self-guided laser-plasma channels, *Nature Photonics* 2, 571 (2008).
- [17] Huang, S.-W. et al. High conversion efficiency, high energy terahertz pulses by optical rectification in cryogenically cooled lithium niobate. *Opt. Lett.* 38, 796 (2013).
- [18] Huang, W. R. et al. Highly efficient terahertz pulse generation by optical rectification in stoichiometric and cryo-cooled congruent lithium niobate. *J. Mod. Opt.* 1–8 (2014).
doi:10.1080/09500340.2013.868547.
- [19] Blanchard, F. et al. Effect of extreme pump pulse reshaping on intense terahertz emission in lithium niobate at multimillijoule pump energies. *Opt. Lett.* 39, 4333 (2014).
- [20] Fülöp, J. A. et al. Efficient Generation of THz Pulses with 0.4 mJ Energy. *Opt. Express* (2014).
- [21] Hebling, J. et al. Optical Manipulation of Relativistic Electron Beams using THz Pulses.
arXiv:1109.6852 1–4 (2010).
- [22] Wong, L. J., Fallahi, A. & Kärtner, F. X. Compact electron acceleration and bunch compression in THz waveguides. *Opt. Express* 21, 9792 (2013).
- [23] Pálfalvi, L., Fülöp, J. A., Tóth, G. & Hebling, J. Evanescent-wave proton postaccelerator driven by intense THz pulse. *Phys. Rev. Spec. Top. - Accel. Beams* 17, 031301 (2014).
- [24] Li, S. & Jones, R. R. Ionization of Excited Atoms by Intense Single-Cycle THz Pulses. *Phys. Rev. Lett.* 112, 143006 (2014).
- [25] Wimmer, L. et al. Terahertz control of nanotip photoemission. *Nature Phys.* 10, 432–436 (2014).

- [26] Emma, P. et al. First lasing and operation of an angstrom-wavelength free-electron laser. *Nature Photon.* 4, 641–647 (2010).
- [27] Thompson, M. et al. Breakdown Limits on Gigavolt-per-Meter Electron-Beam-Driven Wakefields in Dielectric Structures. *Phys. Rev. Lett.* 100, 214801 (2008).
- [28] Hassanein, A. et al. Effects of surface damage on rf cavity operation. *Phys. Rev. Spec. Top. - Accel. Beams* 9, 062001 (2006).
- [29] Hong, K.-H. et al. Generation of 287 W, 5.5 ps pulses at 78 MHz repetition rate from a cryogenically cooled Yb:YAG amplifier seeded by a fiber chirped-pulse amplification system. *Opt. Lett.* 33, 2473–5 (2008).
- [30] Halbach, K. & Holsinger, R.F. (1976). SUPERFISH - a computer program for evaluation of rf cavities with cylindrical symmetry. *Particle Accelerators* 7, 213-222 (1976).

Acknowledgements

We acknowledge Michael Swanwick and Peter R. Krogen for experimental assistance, Eduardo Granados for initial contributions to the project, and William S. Graves and Erich P. Ippen for helpful discussions. This work was supported by DARPA under contract N66001-11-1-4192, by the Air Force Office of Scientific Research under grant AFOSR - A9550-12-1-0499, the European Research Council through Synergy Grant 609920, and the excellence cluster “The Hamburg Centre for Ultrafast Imaging- Structure, Dynamics and Control of Matter at the Atomic Scale” of the Deutsche Forschungsgemeinschaft. L. J. W. acknowledges support from the Agency for Science, Technology and Research (A*STAR), Singapore.

Author contributions

W.R.H., K-H.H., and F.X.K. conceived and designed the experiment. W.R.H. built and performed the experiment with help from E.A.N. and P.D.K. K.R. provided insights to optimize the terahertz source.

E.A.N., K.R., K-H.H., P.D.K., and F.X.K. provided feedback to improve the experiment. W.R.H. developed and performed the simulations with help from E.A.N. and L.J.W. L.J.W. and A.F. performed supporting simulations. W.R.H. and E.A.N. analyzed the data and interpreted the results. W.R.H. wrote the manuscript with contributions from E.A.N. and K.R. and revisions by all. K-H.H., L.Z. and F.X.K. provided management and oversight to the project.

Competing financial interests

The authors declare no competing financial interests.

Materials & Correspondence

Correspondence and requests for materials should be addressed to F.X.K.